

The Impact of Ultraviolet Radiation in High Temperature Space Missions

Claus G. Zimmermann
EADS ASTRIUM
81663 Munich
Germany

Email: claus.zimmermann@astrium.eads.net

Keyword(s): UV radiation, solar cell, high temperature

Abstract

Concentrated ultraviolet (UV) radiation in combination with high temperature was found to constitute an aggressive environment for standard space photovoltaic assemblies. A high intensity, high temperature (HIHT) environment, typical for missions to the inner planets of the solar system like Mercury, characterized by temperatures of 500 K and 11 solar constant irradiance in the UV region below 400 nm, was simulated in vacuum. Independently of the triple junction cell technology used, module degradation up to 20 % in maximum power was observed during several hundred hours of test. Electroluminescence analysis identified discrete top cell shunts close to the cell edge, in particular around the front side contact pads. Cross-sectional transmission electron microscopy performed on several degraded cells revealed an etched contact pad metallization / cap layer interface and more importantly, several 100 nm large, oriented Cu_3P inclusions at the shunted locations. A chemical degradation mechanism is proposed. Short wavelength UV light interacting with polysiloxanes used as module encapsulant produces hydrogen and methyl radicals. With these building blocks an organic acid can be formed on external reaction surfaces like the Ag busbars that simultaneously serve as a source of oxygen. Cu traces present in the Ag segregate to the surface and are transported by this acid to the contact pad of the cell in the liquid phase. This UV induced degradation mechanism is also able to explain the distinctly non-equilibrium surface morphology found on Ag surfaces after HIHT exposure: Ag particles of different aspect ratios, 50–1000 nm in size, including a small fraction of nanorods, had formed on the surface.

1. Introduction

For the success of high intensity, high temperature (HIHT) missions to the inner region of the solar system it is important to understand how the solar array, one of the most exposed subsystems, behaves in this environment. To phrase the question more specifically: Is a stable operation of the photovoltaic assembly (PVA), consisting of the solar cell and its immediate surroundings, possible in a HIHT environment? As a model environment the HIHT conditions typical for the joint JAXA / ESA mission Bepi Colombo to Mercury were chosen. These are characterized by maximum temperatures of 230 °C, combined with 11 solar constants irradiation. Since the ultra-violet (UV) part of the spectrum below 400 nm is assumed to be the most damaging, the focus in this work was to reproduce the solar irradiance in this wavelength regime accurately, while neglecting the longer wavelength part of the spectrum.

2. High temperature UV testing

PVA representative samples were prepared. The carbon fiber structure was replaced by an Al plate, but all sun exposed parts of the PVA were reproduced accurately. The multijunction cell was assembled with a 100 μm thick cerium doped CMX coverglass. A transparent Pt addition cured silicone was used as a coverglass adhesive. Another addition-cured silicone served as laydown adhesive to bond the solar cell assembly to the Kapton surface. The 50 μm thick Kapton foil was in turn bonded with the same adhesive on the Al plate. The electrical interconnection was performed with Ag interconnectors welded to Ag busbars. For external connection, Kapton insulated, Ag plated Cu wires were attached. A photograph of this sample configuration is shown in Fig. 3.

To cover a broad range of technologies, different current multijunction cell technologies were tested, labeled A - D. In addition, the outermost cell surface, the antireflection (AR) coating, which interfaces with the surrounding materials, was varied as well. The standard dual layer $\text{TiO}_x/\text{AlO}_x$ AR coating as well as

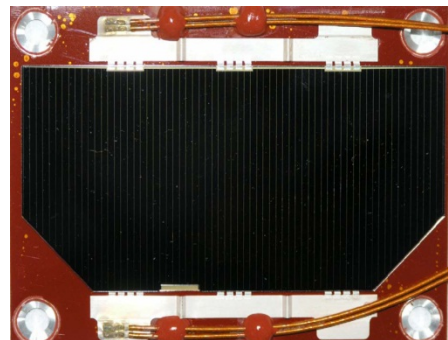


Fig. 3: PVA representative sample layout. The carbon fiber structure was replaced by an Al plate. A Kapton foil was bonded with silicone adhesive containing iron oxide particles to the Al plate, which explains the red color.

pure AlOx and no AR coating were used. Furthermore the spatial distribution of the AR coating was varied. Shadow masking and photolithographic AR structuring can be used to ensure that the welding pads remain free of AR coating. The shadow mask technique leads to a larger AR free area.

Specialized vacuum chambers available at the European Space Research and Technology Center (ESTEC) of ESA were used to simulate the UV high temperature environment. An external array of up to 8 specialized arc discharge lamps produced the UV radiation that entered the chamber through a fused silica viewport. The integrated intensity between 200 and 400 nm was measured and adjusted at the desired number of solar constants. The samples were mounted on a base plate with heating and cooling capacity to reach the desired sample temperatures during test. A liquid nitrogen cooled cold shroud reduced the base pressure to the low 10⁻⁶ Torr range. 3 similar facilities were available at ESTEC and were used in a series of UV tests that accumulated several thousand actual hours of UV exposure. The results of a particular illustrative test are outlined here.

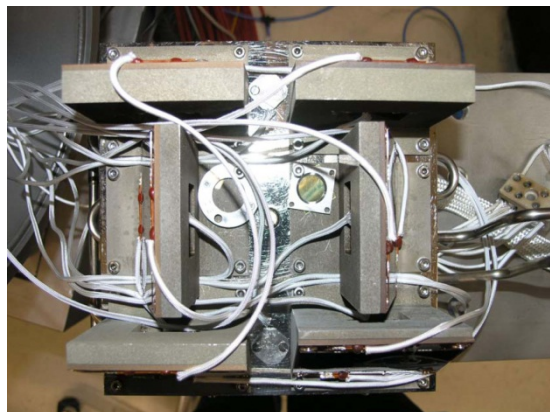


Fig. 4: Test setup for high temperature UV testing under inclined conditions.

Six 8 x 4 cm² sized multijunction solar cells did fit in the same test chamber as illustrated in Fig. 4. To reduce the effective solar irradiance and thus the array temperature, the PVA is often operated under high inclination angles in HIHT missions. This was reproduced in this particular test as well with the help of Al prisms that allowed to position the cell normal at angles α of 60°, 70° and 80° relative to the incident UV radiation. The details of the sample configuration tested are summarized in Table 1. The test was performed at 230 °C and 11 solar constants for two exposure durations of 600 h each. 3 samples were replaced after the first phase by 3 new samples.

Table 1: Maximum power degradation P_{max} in a two phase UV test of 600 h test duration each.

cell	description	α	P_{max} 600 h	$P_{max} + 600$ h
1	cell A, AlOx AR (s)	70°	-2.6 %	-3.5 %
2	cell A, TiOx/AlOx AR (s)	60°	-5.0 %	-7.1 %
3	cell A, w/o AR	80°	-1.8 %	-13.8 %
4	cell C, AlOx AR (s)	70°	-19.0 %	n/a
5	cell B, TiOx/AlOx AR (p)	70°	-9.0 %	n/a
6	cell A, AlOx AR (s)	80°	-8.1 %	n/a
7	cell A, AlOx AR (s)	80°	n/a	-2.2 %
8	cell A, AlOx AR (s)	70°	n/a	-11.7 %
9	cell A, AlOx AR (s)	70°	n/a	-11.9 %

s: shadowmask structuring
p: photolithographic structuring

The changes in maximum power output P_{max} of the cells before and after exposure are summarized in Table 1. The results of this UV test show all typical features of the HIHT degradation corroborated by several similar tests. There is always significant statistical spread in the data, i.e. there are always some cells like cell 1 that degraded by only 3 %, in line with pure darkening in the coverglass adhesive, while other cells degraded in the \approx 10 % range. In some cases degradations up to 20 %, as for cell 4, were measured. This performance degradation was not related to the cell technology used. The behavior of cell 3, which was stable in the first phase, but started to degrade in the second phase was observed only in this instance.

In order to identify the root cause of this unexpected degradation, a set of specifically designed tests was carried out. They contained the triple junction solar cell and only a limited number of material combinations. Worst case test conditions of 230 °C and 11 solar constants under perpendicular incidence were chosen. The nominal test duration was 400 h. Each test included an identical set of six 8 x 4 cm² sized solar cells. Cells 1 and 2 were B type cells with a photolithographic TiOx/AlOx AR coating, cell 3 was an A cell with a shadow mask TiOx/AlOx coating, cells 4 and 5 A type cells with an AlOx shadow mask coating, and cell 6 represented an A cell completely without AR coating. Only in the first test, the bare cell test, cell 4 was replaced by a D type cell with shadow mask TiOx/AlOx AR coating and cell 5 was another A cell with TiOx/AlOx coating.

In the bare cell test (test 1), the cells were mounted with the help of 5 small magnets embedded in the Al sample plate. A fused silica window, completely UV transparent, was placed on the cell and supported the corresponding magnets applied on top of the cell. The frontside cell interconnector was welded directly onto an Ag foil that protruded from underneath the cell thus ensuring short circuit conditions during test. No other PVA material was present in the test. On cells 2, 3, 5 and 6 a CMX coverglass was placed underneath the fused silica window to expose the cell surface to the realistic, filtered UV radiation. The first additional PVA material investigated in test 2 was the coverglass adhesive. 100 μ m thick CMX coverglasses were bonded onto the cell

with a transparent silicone adhesive. The remainder of the sample configuration was identical to the bare cell test. In the next test group, test 3, a silane primer was applied in addition on the cell rearside. The final three testgroups all contained the laydown silicone adhesive. They all resembled the sample layout illustrated in Fig. 1, including the Kapton foil, Ag busbars and Kapton insulated wiring. Three different combinations were tested. Test 4 used in addition coverglass adhesive, but no primer on the cell rearside, test 5 the silane primer, but no coverglass adhesive and test 6 used neither coverglass adhesive nor primer. In the last two configurations the cell was protected by a 100 µm CMX coverglass, that was attached with the help of the fused silica / magnet configuration.

Table 2: Relative P_{max} degradation of different cell / PVA material combinations during a 400 h, 11 solar constant UV irradiation at 230 °C

cell	Description	test 1: bare cell	test 2: only coverglass adhesive	test 3: coverglass adhesive + primer	test 4: coverglass + laydown adhesive	test 5: laydown adhesive + primer	test 6: only laydown adhesive
1	cell B, TiOx/AlOx AR (p)	0.9	-2,2	-3,4	-8,6	-5.1 / -9,2**	-4,9
2	cell B, TiOx/AlOx AR (p)	-0.9	-3,3	-5,3	-4,7	-5.2 / -9,4**	-9,6
3	cell A, TiOx/AlOx AR (s)	1.9	-12,1	-11,0	-4,7	--	--
4	cell A, AlOx AR (s)	0.9*	-4,3	-2,6	-2,8	-4.1 / -7,4**	-7,6
5	cell A, AlOx AR (s)	--	-4,5	-4,2	-2,6	-7.3 / -13,3**	-9,7
6	cell A, no AR	0.4	-4,2	-4,7	-2,5	-9.1 / -16,5**	-8,5
* cell replaced by cell D, TiOx/AlOx AR (s) -- cell mechanically damaged during test ** extrapolated linearly from 240 h to 400 h s: shadowmask structuring p: photolithographic structuring							

The change in performance is summarized in Table 2. Several important conclusions can be drawn from these tests. First and foremost, it can be concluded from test 1 that bare cells do not degrade, despite the fact that the test duration was shortened to 200 h in this case. Degradation, however, started to occur as soon as silicones were present, either in their function as laydown or as coverglass adhesive. The remaining PVA materials did not appear to make any difference. Likewise, the degradation showed no correlation to the cell type and AR configuration used. A pronounced difference, however, could be observed between the test groups in which the coverglass was bonded with silicone adhesive, i.e. test 2, 3 and 4, and the test groups 5 and 6 which featured comparably unprotected cell surfaces. The average degradation in the latter group is $\approx 8\%$, twice as high than the average degradation observed in the first group. It has to be noted that the duration of test 5 was only 240 h, therefore the results were extrapolated linearly to 400 h.

This implies that the coverglass adhesive can both act as a source of the degradation as in tests 2 and 3, but at the same time also function as a barrier against it. This barrier seems to limit the degradation to 4 % in most cases, but in every test there was at least one cell where it apparently failed to work and the cell degraded as much as the unprotected cells in tests 5 and 6. It was verified experimentally that photovoltaic assemblies according to Fig. 3 did not degrade upon exposure to high temperature alone, without the presence of UV light. The degradation mechanism is thus linked to a photochemical reaction of the silicones initiated by UV light. Coverglass as well as laydown adhesive are both methyl-phenyl polysiloxanes, which have an absorption maximum at $\approx 260\text{ nm}$ [1]. Only this short wavelength light can initiate photochemical processes. For longer wavelength UV light they are highly transparent and no energy is absorbed. This explains the partly protective nature of the coverglass adhesive. The adhesive behind the coverglass is protected from UV light below 325 nm, since this part of the spectrum is absorbed in the glass itself. Only silicones which are exposed to the UV irradiation directly either at the cell edge or at reaction surfaces external to the cell can contribute to the degradation.

3. Discussion

3.1 Microanalysis

The IV curve of cell 4 according to Table 1 is shown in Fig. 5, which exhibits the typical features of a highly degraded cell. The IV curve changes its slope around 1.5 V, which is indicative of an ohmic shunt in one subcell. The fact that V_{oc} is reduced as well indicates the presence of an additional diode like shunt component. Electroluminescence imaging is ideally suited to identify the location of shunts both spatially as well as in depth [2,3]. The middle cell electroluminescence image of cell 4, illustrated in Fig. 6, shows bright half moon shaped areas around the three frontside contact pads. The top cell electroluminescence image of cell 4 was exactly

inverse, with dark areas appearing at the contact pads. This is the signature of a shunt located in the top cell. The intensity of the half moon shaped areas increases towards the cell edge, as highlighted by the inset in Fig. 6. The shunts, which act as a current sink and affect the electroluminescence image in this characteristic fashion, thus have to be located very close to the cell edge.

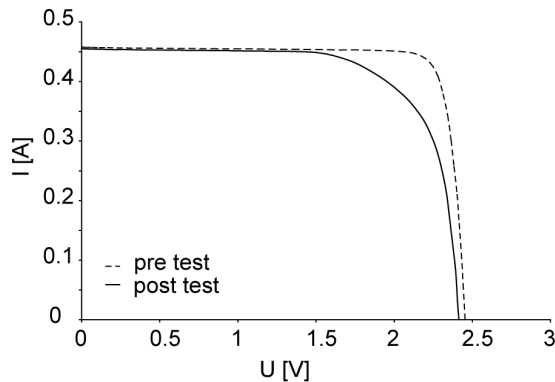


Fig. 5 : IV curve of cell 4 in Table 1 before and after test showing a large fill factor degradation

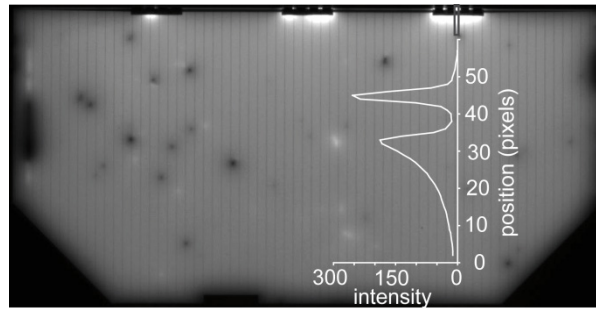


Fig. 6 : Middle cell electroluminescence image of cell 4 according to Table 1. The inset shows an intensity profile along the area indicated on the right contact pad.

To be able to analyze the shunts with standard analytical techniques, their exact position had to be determined with orders of magnitude better resolution than used in Fig. 6. For this investigation, a degraded cell (cell 6 from test 6 according to Table 2) without coverglass adhesive was chosen. The interconnector fingers at one contact pad were cut at the busbar and bent backwards. With a specialized electroluminescence setup [3], discrete shunts were located in the approximately 30 μm wide active cell region between the contact pad and the cell edge. Since the electroluminescence image had a μm resolution the position of the shunts could be identified with sufficient accuracy in a scanning electron microscopy (SEM) image acquired from the same area. A typical example is shown in Fig. 8. At discrete positions, always correlated to the location of the shunts in the electroluminescence image, a foreign substance is present at the edge of the contact pad. It appeared to be creeping from the contact pad onto the cell and had the morphological appearance of a dried liquid. Similar observations at the outermost cell edge, also highlighted in Fig. 8, further strengthen this observation. On untested samples similar areas were never observed.

At the most severe shunt of cell 6 from test 6, a cross sectional sample was prepared by focused ion beam (FIB) processing. The sample was further thinned to electron transparency and imaged in a transmission electron microscope (TEM), as shown in Fig. 7. The top cell region, extending about 2 μm underneath the contact pad is shown in Fig. 7a. The area highlighted in red is created as a result of the cap etch step during cell manufacturing and not test related. Three test related features, however, could be observed: i) The top cell surface is etched locally. The etching starts at the position where the foreign substance touches the top cell surface and proceeds underneath the contact pad. ii) Within the top cell surface, shown in higher magnification in Fig. 7b, Cu_3P inclusions are found as confirmed by the energy dispersive X-ray analysis plotted in Fig. 7c. These Cu_3P inclusions, next to the etching of the top cell, sufficiently explain the electrical degradation of the cell. They are

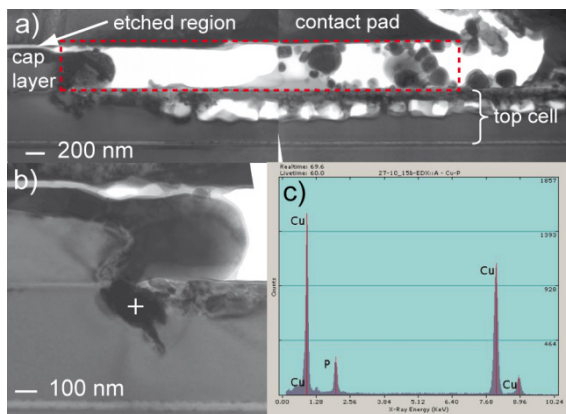


Fig. 7 : a) TEM cross-section through a shunted area of cell 6 from test 6. The area highlighted in red is caused by the cap etch process during cell manufacturing. A higher magnification image shown in b) reveals inclusions in the top cell which are identified by EDX measurements (c) as Cu_3P .

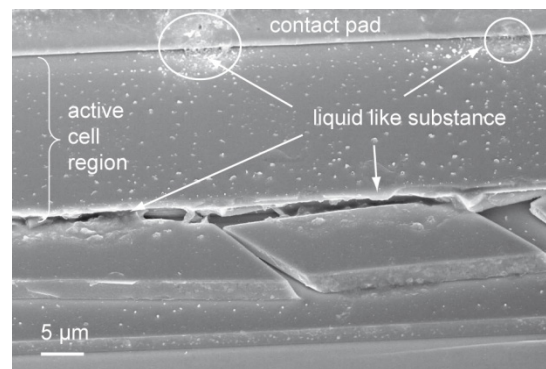


Fig. 8 : Scanning electron microscope (SEM) image of the outermost active cell region located underneath an interconnector finger. The shunted cell locations are highlighted by a circle.

both considerably larger than the top cell emitter thickness. iii) Another feature visible in Fig. 7a is the underetching that developed between the contact pad and the GaAs cap layer. By peeling off part of the contact pad a SEM analysis confirmed that this underetching occurs to a depth of approximately 5 μm , not only at positions where Cu_3P shunts had developed, but along the entire contact pad length.

3.1 Degradation mechanism

An explanation of the detailed failure mechanism is beyond the scope of this paper. Only a brief summary, albeit without the possibility to present all supporting facts [4], can be given here. The root cause test unambiguously proved that a photochemical reaction of silicones, initiated by short wavelength UV light, is essential for the degradation. The microanalysis revealed that cap as well as top cell material at the cell edge in front of the welding pad is etched away in the degraded cells. This is only possible in a liquid phase, with the cell interconnector serving as the transport pathway. This also explains why some cells encapsulated with coverglass and coverglass adhesive are affected as well. Even in this case a transport path along the interconnector can exist in some cells if the coverglass adhesive does not seal the interconnector completely. As cause of the ohmic shunts, Cu_3P inclusions in the top cell have been identified. Since Cu is an element that is not present in the bare cell at all, it has to be transported there as well, presumably by the same liquid-like transport mechanisms.

The only component in the PVA assembly that contains Cu is the Ag busbar and the Ag interconnectors. 0.1 % Cu is present there intentionally in the bulk to improve the mechanical properties of pure Ag by solid solution hardening. Close to the surface, however, Cu is enriched, since this is energetically favorable. The Ag busbar was analyzed by XPS in sputter depth profiling mode. 1-2 % Cu was detected in the first 5 nm. In addition, in a 30 nm layer underneath the surface, an average oxygen content of 10 % was found in the Ag. Finally on top of the Ag surface, a 6 nm thick layer of siloxane fragments was found. This is the result of the outgassing of short chain length silicone fragments in the HIHT test conditions. A CaF_2 witness plate contained a similar amount of silicone.

The Ag busbar is also fully exposed to the entire UV wavelength spectrum. Methyl phenyl polysiloxanes irradiated by short wavelength UV light provide hydrogen and methyl radicals [1]. Together with the oxygen contained in the Ag close to the surface, all building blocks for an organic acid are present. Based on the interaction probability, the formation of the simplest species like formic acid or acetic acid seems to be most likely. Such substances can be present as nm thick surface films even at temperatures of 200 $^\circ\text{C}$ and vacuum [5]. Alternatively, simple aromatic carboxylic acids such as benzoic acid, with a much higher boiling point, might form through the abstraction of a phenyl group. Due to the minimal amount of these substances found, they could not be identified directly by analytical techniques. They are, however, a likely explanation for the etching found on the degraded cell. Since Cu containing carboxylic acids are also easily formed, they appear to be also the transport vehicle for Cu to the top cell at the same time. The delivery of Cu to the cell in such an organic form is also well in line with the formation of oriented Cu-P inclusions. For any other delivery method it is very hard to explain the formation of such inclusions in an oriented fashion at the comparatively low test temperatures. A more detailed account of this proposed degradation mechanism can be found in Ref. [4].

The central nature of the busbar in this UV-high temperature cell degradation is further supported by the microstructure of the Ag surface after test. In Fig. 9a a SEM image of the Ag surface is shown. It presents a distinctly non-equilibrium surface morphology: Nanoparticles from 50 to 1000 nm in size have formed, together with a small fraction of nanorods. These features, although consisting of pure Ag, are only loosely attached to the surface and can be easily removed by an adhesive tape. As shown Fig. 9b, they are sitting on top of pits in the Ag

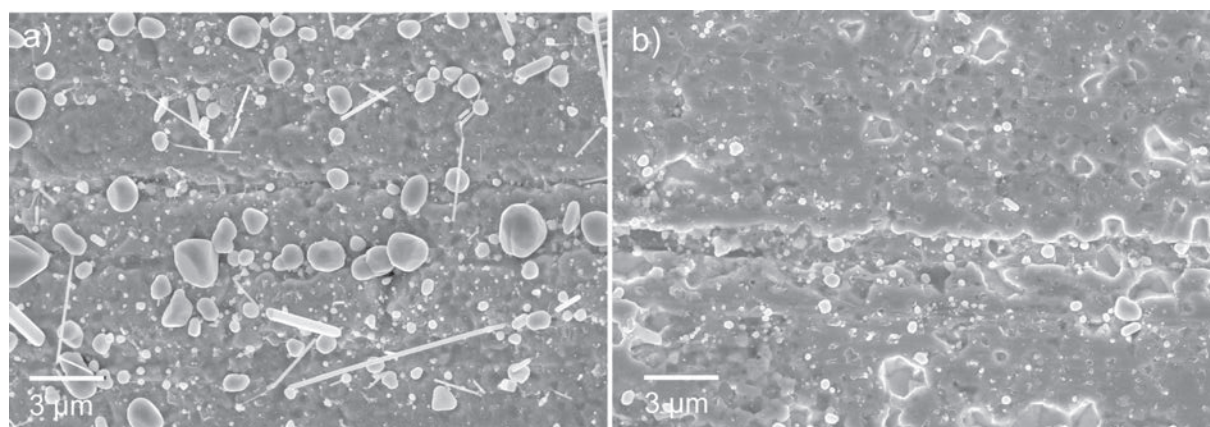


Fig. 5: a) SEM image of the Ag busbar surface morphology after UV testing. Up to micron-sized Ag particles are present on the surface. They can be easily removed by an adhesive tape. b) Pits in the Ag surface now become visible that were obscured by the particles originally. The pits appear to be aligned with Ag grains. Note that images a) and b) do not show an identical area.

surface, which are aligned with grain boundaries in the polycrystalline Ag. As reported in detail in [6], this morphology can be explained by the same photochemical reaction of the silicone layer on top of the busbar. The hydrogen radicals produced in this fashion diffuse very rapidly into the silver along grain boundaries. In pre-existing voids they form water molecules together with the oxygen already present in the Ag. The hydrostatic pressure created by this intrinsic water vapor drives the diffusion of Ag atoms to the surface. Modeling this process [6] results in slightly less than 400 h that are required for a 1 μm sized void with an internal pressure of 9 MPa during growth to form, in line with the experimental timescales.

4. Conclusion

Silicones, which are under standard geostationary environmental conditions a very inert substance, can exhibit a quite different behavior in a HIHT environment. Under short wavelength UV irradiation, reactive hydrogen and methyl radicals are released, which are the source of their aggressive nature. Current triple junction solar cells are nanostructure devices in one dimension, with a top cell emitter thickness below 100 nm. Therefore they are quite sensitive components that can be easily affected. Only a very small amount of Cu is required to create the observed Cu_3P shunts. By using a slightly modified cell design [4], a complete encapsulation of the cell is achieved and a stable operation in a HIHT environment is possible.

References

- [1] S. Siegel, R. J. Champetier and A. R. Calloway, "Quantum efficiency of the 2357 Å photolysis of a mixed phenyl-methyl polysiloxane," *J. Polymer Science* **4**, 2107 (1966)
- [2] C. G. Zimmermann, "Utilizing lateral current spreading in multijunction solar cells: an alternative approach to detecting mechanical defects," *J. Appl. Phys.* **100**, 023714 (2006)
- [3] C. G. Zimmermann, "Performance mapping of multijunction solar cells based on electroluminescence," *Electron Device Letters* **30**, 825 (2009)
- [4] C. G. Zimmermann, C. Nömayr, M. Kolb and A. Rucki, "A mechanism of solar cell degradation in high intensity, high temperature space missions" *Prog. Photovolt: Res. Appl.* 1195 (2011)
- [5] H. G. Tompkins and D. L. Allara, ""The study of the gas - solid interaction of acetic acid with a cuprous oxide surface using reflection-absorption spectroscopy," *Colloid and Interface Science* **49**, 410 (1974)
- [6] C. G. Zimmermann, "Surface modification by subsurface pressure induced diffusion," *Appl. Phys. Lett.* 100 (2012) 04